Non-ultraviolet-based patterning of polymer structures by optically induced electrohydrodynamic instability

Wang, Feifei; Yu, Haibo; Liu, Na; Mai, John D.; Liu, Lianqing; Lee, Gwo-Bin; Jung Li, Wen

Published in:
Applied Physics Letters

Published: 18/11/2013

Document Version:
Final Published version, also known as Publisher's PDF, Publisher's Final version or Version of Record

Published version (DOI):
10.1063/1.4830001

Publication details:
Wang, F., Yu, H., Liu, N., Mai, J. D., Liu, L., Lee, G.-B., & Jung Li, W. (2013). Non-ultraviolet-based patterning of polymer structures by optically induced electrohydrodynamic instability. *Applied Physics Letters*, *103*(21), Article 214101. https://doi.org/10.1063/1.4830001

Applied Physics Letters

Non-ultraviolet-based patterning of polymer structures by optically induced electrohydrodynamic instability

Cite as: Appl. Phys. Lett. **103**, 214101 (2013); https://doi.org/10.1063/1.4830001
Submitted: 08 July 2013 • Accepted: 23 October 2013 • Published Online: 18 November 2013

Feifei Wang, Haibo Yu, Na Liu, et al.

Non-ultraviolet-based patterning of polymer structures by optically induced electrohydrodynamic instability

Feifei Wang,[1,2] Haibo Yu,[1] Na Liu,[1,2] John D. Mai,[3] Lianqing Liu,[1,a)] Gwo-Bin Lee,[4] and Wen Jung Li[1,3,b)]

[1]*State Key Laboratory of Robotics, Shenyang Institute of Automation, Chinese Academy of Sciences, Shenyang 110016, China*
[2]*University of Chinese Academy of Sciences, Beijing 100049, China*
[3]*Department of Mechanical and Biomedical Engineering, City University of Hong Kong, Kowloon, Hong Kong*
[4]*Department of Power Mechanical Engineering, National Tsing Hua University, Hsinchu 30013, Taiwan*

(Received 8 July 2013; accepted 23 October 2013; published online 18 November 2013)

We report here an approach to rapidly construct organized formations of micron-scale pillars from a thin polydimethylsiloxane (PDMS) film by *optically induced electrohydrodynamic instability* (OEHI). In OEHI, a heterogeneous electric field is induced across two thin fluidic layers by stimulating a photoconductive thin film in a parallel-plate capacitor configuration with visible light. We demonstrated that this OEHI method could control nucleation sites of pillars formed by electrohydrodynamic instability. To investigate this phenomenon, a tangential electric force component is assumed to have arisen from the surface polarization charge and is introduced into the traditional perfect dielectric model for PDMS films. Numerical simulation results showed that this tangential electric force played an important role in OEHI. © *2013 AIP Publishing LLC*. [http://dx.doi.org/10.1063/1.4830001]

Polymer patterns of nano- to micrometer size imbue distinctive properties to a substrate. These unique properties can be useful in electronics, optoelectronics, cell and tissue engineering, and surface science.[1] Strategies used to pattern polymers include photolithography, microcontact printing,[2] block copolymer self-assembly,[3] and electrohydrodynamic instability (EHDI)-induced polymer patterning.[1,4,5]

EHDI appears when an electric field overcomes surface tension in thin films[4] that are spun onto a lower electrode and separated from an upper electrode by a medium such as air,[6,7] another polymer,[8] or an ionic liquid.[9] Traditionally, pillars generated by EHDI self-organize into hexagonal arrays[4,5,10] with a predictable spacing.[11] The pillars appear randomly[12] in homogeneous electric fields or assemble according to the protruding relief of the upper electrode.[5,6,12,13] Theoretical analysis has shown that chemically heterogeneous and patterned substrates can also be used to induce spatial electric field distributions and obtain desired pillar arrays.[14,15] Grilli *et al*. exploited the pyroelectric effect to generate an electrical potential that could induce variations in the wettability of a lithium niobate substrate to grow microstructures on a polydimethylsiloxane (PDMS) film.[16] However, a common problem of the aforementioned methods for organizing pillars into desired arrays is that the electrode or substrate needs to be patterned first, which adds complexity to the total process.

We present here experimental results from using visible light generated by a projector to induce heterogeneous spatial distributions of an electric field between two parallel electrodes by stimulating a photosensitive layer on the lower electrode. This heterogeneous electric field can be further used to control the nucleation sites of pillars induced by EHDI in a process we call *optically induced electrohydrodynamic instability* (OEHI). In this letter, the experimental setup and results are first presented. Then, a theoretical model is derived and solved numerically using a finite element method software to qualitatively explain this OEHI phenomenon.

The schematic of the OEHI-based fabrication process is given in Figure 1. First, PDMS (Dow Corning, Sylgard-184) was spin-cast onto a hydrogenated amorphous silicon (a-Si:H)-covered ITO-glass [Fig. 1(a)]. Then, this surface was combined with another ITO-glass as an upper electrode, which was modified with a monolayer of the mold release agent trichloro(1H,1H,2H,2H-perfluorooctyl)silane (97%, Sigma-Aldrich) through vapor deposition,[9] to assemble a parallel-plate capacitor configuration. Our experimental results showed that this surface modification could effectively suppress pillar movement when EHDI occurs at the interface of the PDMS and the air. The gap between the initially flat polymer film and the upper electrode was

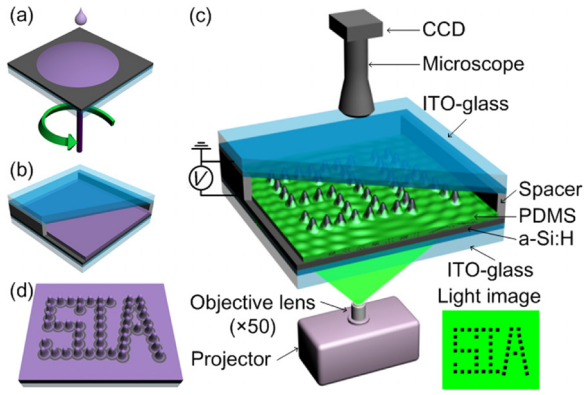

FIG. 1. Experimental process used in OEHI, with illustration of the experimental setup and structure of the chip used to generate OEHI.

a)For hardware system configuration, contact: lqliu@sia.cn
b)For optically-induced electrohydrodynamic instability, contact: wenjli@cityu.edu.hk

maintained by a spacer (i.e., a layer of aluminum foil or other thin film) [Fig. 1(b)]. After pre-curing the PDMS film at a set temperature of 130 °C to help adjust the viscosity of PDMS and to circumvent the problem of coarsening/ripening,[17] the assembled chip was placed between a digital projector (VPL-F400X, Sony, Japan) and an optical microscope (Zoom 160, Optem, USA). The OEHI phenomenon occurred immediately when the projector and a voltage source (Keithley 2410) were simultaneously turned on [Fig. 1(c)]. After solidifying the PDMS at 130 °C for 20 min, pillars organized in the desired distribution were obtained [Fig. 1(d)].

When illuminated by a light image with a uniform grid, two typical pillar arrays were obtained, as shown in Figs. 2 and 3(b). The pillars in Fig. 2 appeared in the dark area of the light grid (see the inset of Fig. 2). The two different sizes of structures shown in Fig. 3(b) were formed in different time steps. The bigger pillars grew in the dark areas first, which was similar to the generation of structures in Fig. 2. After a few seconds, the smaller pillars appeared in the illuminated areas. Thus, one could create the formation of the smaller structures shown in Fig. 3 by controlling the duration of applied voltage. We also have experimentally validated that the ratio of initial film thickness, the distance between the upper and lower electrodes, the electric field intensity (which could be used to change the diameter of pillars), the center-to-center spacing of the dark areas all had significant influence on the final results. For example, experimental results show that the pillar diameter will increase if the polymer film thickness is increased.[18] However, much more detailed experiments need to be performed before a conclusive remark on controlling the pillar size and nucleation sites can be provided. Sample AFM-scanned profiles of the two types of structures described above are shown in Fig. 4.

To further demonstrate the ability of OEHI to assemble pillars into arbitrary patterns, we used patterned projected light/dark areas to organize pillars into the word "SIA" [Fig. 5(a)] and into concentric circles [Fig. 5(c)]. As in the uniform grid case, the pillars grew exactly in the non-illuminated areas [Figs. 5(b) and 5(d)], which verified that the OEHI could pattern pillars into ordered arrays, and could also be used to disrupt the intrinsic wave propagation, i.e., the characteristic wavelength of EHDI.

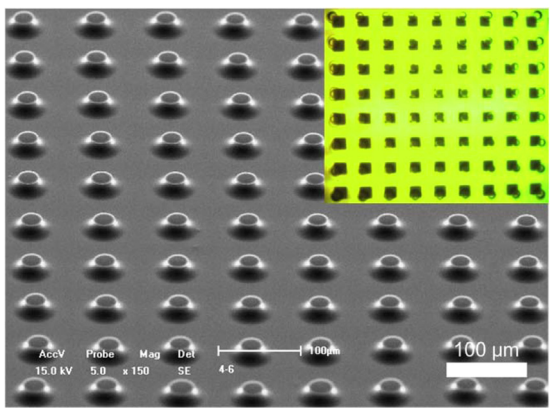

FIG. 2. SEM image showing that pillar array structures were obtained when a light image (inset) of a uniform grid was used to induce OEHI. The inset shows the processed optical microscope image, which was obtained within 54 s. Barrel distortion appeared in the projected area due to optical aberrations. Experimental parameters: ~1.75 μm PDMS film, measured by an atomic force microscope (AFM, D3100, Veeco, Inc.), was pre-cured for 2 min; an applied voltage of 190 V across ~10 μm gap.

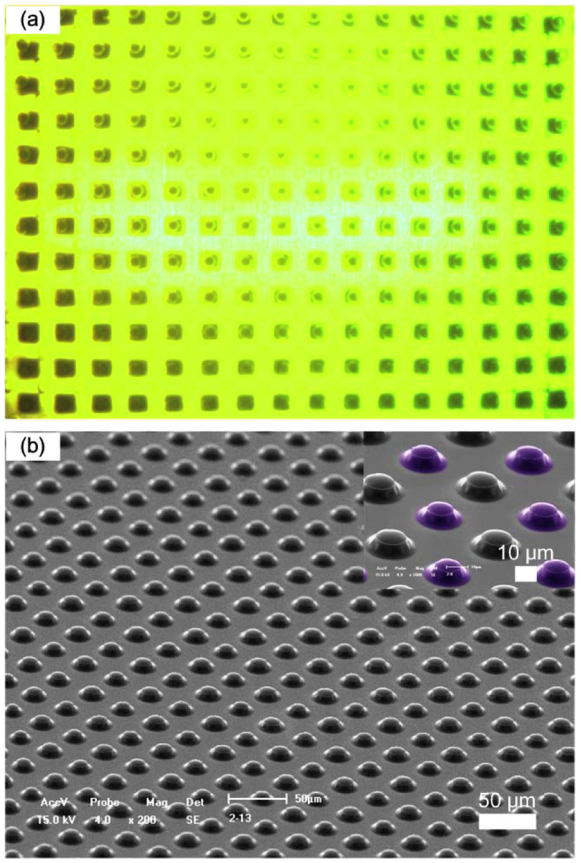

FIG. 3. (a) The projected optical microscope image that was taken at 16 s. (b) The SEM image, demonstrating that another size of pillar array structures, could be obtained when a light image of uniform grid was used, i.e., larger size structures formed in the dark areas of the projected image while smaller size structures formed in the bright areas (The inset SEM image shows color-enhanced smaller size structures). Experimental parameters: ~1.02 μm PDMS film was pre-cured for 2 min; an applied voltage of 260 V across ~5 μm gap (enhanced online) [URL: http://dx.doi.org/10.1063/1.4830001.1].

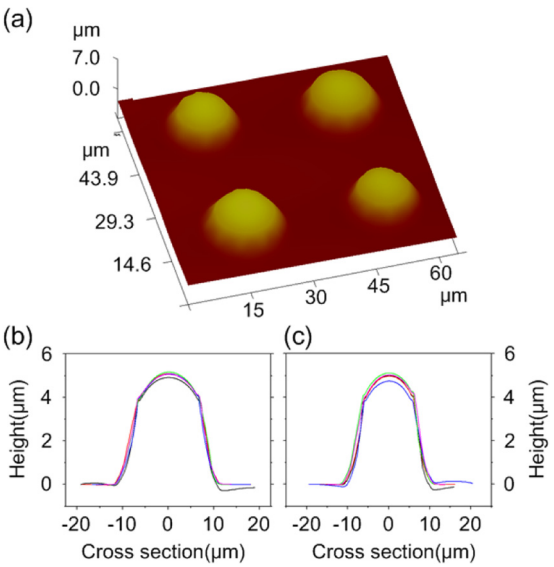

FIG. 4. (a) AFM scanned images showing the two different sizes of the pillars shown in Fig. 3(b). Height information shown in (b) and (c) correspond to the bigger and smaller (purple structures in the inset of Fig. 3(b)) pillars, respectively.

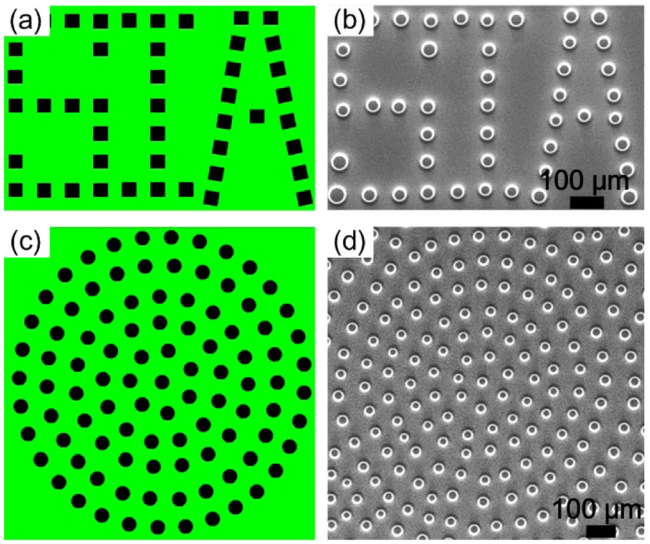

FIG. 5. (a) and (c) The original images as drawn on a computer screen. (b) and (d) show the SEM images of PDMS pillars organized into the letters "SIA" (**S**henyang **I**nstitute of **A**utomation) and into concentric circles by the OEHI-induced heterogeneous electric field. The spacer height, pre-cure time, applied voltage, and initial film thickness used to generate the structures shown in (b) and (d) were ~10 μm, 2 min, 190 V and ~1.75 μm, respectively (enhanced online) [URL: http://dx.doi.org/10.1063/1.4830001.2].

The theory explaining EHDI which is induced by perpendicular electric fields has been widely studied.[7,11] However, a theoretical model has not been well established for surface instability induced by an in-plane electric field. In OEHI, where normal and tangential electric field components simultaneously exist, the condition could be more complex. In order to account for the synergistic effect of normal and tangential electric fields in OEHI, and considering that PDMS behaves as a perfect dielectric,[19] we modified the traditional perfect dielectric model by introducing a surface polarization charge, which is induced by a normal electric field that tolerates a tangential electrical force when a tangential electric field exists. We discuss below a theoretical formulation to possibly explain the generation of interfacial instability of two fluids using optically-induced heterogeneous electric field.

The two fluids defined in Fig. 6 are assumed to be incompressible Newtonian fluids, each with a viscosity of μ_i, $i = 1, 2$. The surface evolution for a thin Newtonian film can be derived from the continuity and the Navier-Stokes equations and then simplified using a long-wave approximation. When Fluid 1 is air and Fluid 2 is a polymer, the viscosity of the upper fluidic layer is negligible, and the spatial and temporal evolution of the interface $h(x,t)$ can be described as[20]

$$\mu_2 \frac{\partial h}{\partial t} + \frac{1}{2}\frac{\partial T h^2}{\partial x} - \frac{1}{3}\frac{\partial}{\partial x}\left[h^3 \frac{\partial N}{\partial x}\right] = 0, \tag{1}$$

where N and T are the normal and tangential stresses acting on the interface, respectively. The normal stress N is mostly due to the normal component of the destabilizing electric field force (N_{elec}) and the stabilizing surface tension (the van der Waals interactions and other intermolecular interactions are not considered here). Namely,

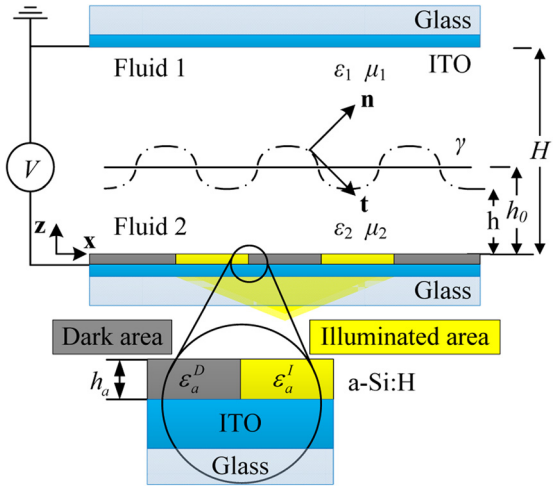

FIG. 6. Schematic diagram illustrating the configuration of the chip used to *optically induce electrohydrodynamic instability* and the Cartesian coordinate system used for the theoretical analysis. Fluid 1 is air and Fluid 2 is PDMS in this figure.

$$N = N_{elec} - \gamma \frac{\partial^2 h}{\partial x^2}, \tag{2}$$

where γ is the interfacial tension. A temperature gradient induced by light and which has an influence on the surface tension could also cause a thermocapillary flow. The influence of thermocapillary flow, which maybe also influence the position of the nucleation sites, is under investigation by our team and will be reported after more extensive experimentation.

The Maxwell stress tensor, which corresponds to the Korteweg-Helmholtz polarization force density, for the interaction between the incompressible liquid and the electrostatic field, which will affect the fluid through the interface, can be expressed as[11,21,22]

$$\mathbf{m} = \varepsilon_0 \varepsilon \left(\mathbf{EE} - \frac{1}{2}\mathbf{E}\cdot\mathbf{E}\boldsymbol{\delta} \right), \tag{3}$$

where $\boldsymbol{\delta}$ is the identity matrix and ε is the dielectric constant of polymer (Fluid 2 here).

The normal component of the Maxwell stress at the interface is[21]

$$N_{elec} = \mathbf{n}\cdot\mathbf{m}\cdot\mathbf{n}, \tag{4}$$

where $\mathbf{n}$ is the unit normal vector to the interface as shown in Fig. 6.

The electric field in Fluid i is given by $\mathbf{E}_i = -\nabla\psi_i$. The tangential component of the Maxwell stress at the interface is zero because there is no net interfacial free charge accumulating at the interface in the perfect dielectric model. As the bulk of the fluid has no net free charge, the governing equation for the electric potential ψ_i in Fluid i is

$$\nabla^2 \psi_i = 0. \tag{5}$$

The boundary conditions are[11,21]

$$\begin{aligned} &\psi_1 = 0 \quad \text{at} \quad z = H, \\ &\psi_2 = \psi_b \quad \text{at} \quad z = 0, \\ &\psi_1 = \psi_2, \quad \varepsilon_0\varepsilon_1 \mathbf{E}_1\cdot\mathbf{n} - \varepsilon_0\varepsilon_2\mathbf{E}_2\cdot\mathbf{n} = 0 \quad \text{at} \quad z = h, \end{aligned} \tag{6}$$

where ψ_b is the potential at $z = 0$; $\varepsilon_i (i = 1, 2)$ is the dielectric constant of Fluid i; since Fluid 1 is air, ε_1 is one; and ε_0 is the permittivity of a vacuum.

We next turn to the equations for the tangential stress T. A lateral/tangential electric field always exists in the liquid layer, because the light excitation induces changes in the electrical properties of the a-Si:H layer. The surface polarization charge density σ_{sp}, which result in the discontinuity of the normal component of an electric field at the interface (even with no free charge accumulated) and which is related to the normal component of the electric field, is[23,24]

$$\sigma_{sp} = -\varepsilon_0 (E_{2n} - E_{1n}), \tag{7}$$

$$E_{in} = \mathbf{E}_i \cdot \mathbf{n}, \tag{8}$$

where E_{in} is the normal electric field intensity component in the Fluid i. A tangential stress (due to the electrical force), T_{elec}, is exerted on the interface by this surface polarization charge in the presence of the tangential electric field. Then, the tangential stress T can be expressed as

$$T = T_{elec} = \sigma_{sp} E_{2t}, \tag{9}$$

$$E_{it} = \mathbf{E}_i \cdot \mathbf{t}, \tag{10}$$

where E_{it} is the lateral component of the electric field in Fluid i at the interface; $\mathbf{t}$ is the unit tangent vector to the interface as shown in Fig. 6.

The capacitance (C) of the composite layer (i.e., a "composite" layer consisting of the photoconductive amorphous silicon and the two fluidic layers) can be expressed as capacitors in series[14]

$$\frac{1}{C} = \frac{1}{C_a} + \frac{1}{C_{F1}} + \frac{1}{C_{F2}}, \quad \text{where} \quad C_a = \frac{\varepsilon_0 \varepsilon_a A}{h_a},$$
$$C_{F1} = \frac{\varepsilon_0 \varepsilon_1 A}{H - h}, \quad \text{and} \quad C_{F2} = \frac{\varepsilon_0 \varepsilon_2 A}{h}. \tag{11}$$

Here C_a, C_{F1}, and C_{F2} are the capacitances of the a-Si:H of thickness h_a, Fluid 1 of thickness $H - h$ and Fluid 2 of thickness h, respectively; ε_a is the permittivity of the a-Si:H, which when illuminated or non-illuminated is expressed as ε_a^I and ε_a^D, respectively. Then, the potential at $z = 0$ can be expressed as

$$\psi_b = \frac{C_a V}{C_a + \dfrac{C_{F1} C_{F2}}{C_{F1} + C_{F2}}} = \frac{\varepsilon_a \left[\varepsilon_2 H + (\varepsilon_1 - \varepsilon_2) h\right] V}{\varepsilon_a \left[\varepsilon_2 H + (\varepsilon_1 - \varepsilon_2) h\right] + \varepsilon_1 \varepsilon_2 h_a}, \tag{12}$$

where V is the DC voltage applied between the two electrodes.

The appearance of pillars first in the dark areas was unexpected but could be explained by the following analysis. As the permittivity of the a-Si:H increases when it is irradiated by light,[25] an increase of ψ_b in Eq. (12) is induced, and the electric field is thus enlarged in the illuminated areas. Similarly, for a physically patterned electrode, the protruding areas, i.e., the areas with a larger electric field, are the areas in which the pillars normally appear. On the other hand, Srivastava *et al.* performed a theoretical analysis using a lubrication approximation, which pointed out that pillars grow in areas with a large permittivity where a larger electric Maxwell stress exists.[14] This finding is contrary to our experimental results. A possible reason is that in the lubrication approximation, the lateral electric field component and the tangential component of the stress at the interface are negligible. However, these lateral and tangential components can play an important role in EHDI in some specific situations, i.e., when $(H - h_0)/H \approx 1$ and $H/L \gg 1$, where L is the electrocapillary length.[6]

Using the theoretical models discussed above, a multiphysics simulation was conducted using a commercial finite element method (FEM) software (COMSOL 4.3) to qualitatively understand the phenomenon of OEHI. This simulation was conducted by using the hydrodynamic module, which contains the fundamental equations used to deduce Eq. (1), i.e., the continuity equation, the Navier-Stokes equations, and hydrodynamic related boundary conditions, the electrostatic module, and the moving mesh module of COMSOL. The hydrodynamic model and the electrostatic module were connected by N_{elec} and T_{elec}, which were calculated using Eqs. (4) and (7)–(12). Fig. 7 shows the simulation result for a projected image of a uniform grid as shown in the insets of Figs. 2 and 3(a). The color table in Fig. 7 represents the distribution of voltage in the PDMS film and the air layer.

The normal component of the Maxwell stress (N_{elec}), which is marked with blue arrows, has a difference $((Maximum - Minimum)/Minimum)$ of 4.97% for illuminated areas (where the maximum value appeared) and dark areas (where the minimum value appeared). The tangential electric force, T_{elec}, which is colored green, points toward the dark areas from the illuminated areas. Without this tangential electric force, the initial uniform polymer film will generate "Taylor cones," which would finally evolve into pillars, in the illuminated areas with larger N_{elec}. The simulation result also indicates that the velocity of the PDMS fluidic layer has an upward component in the dark areas and a downward component in the illuminated areas. This information of the direction of the velocity was consistent with the experimental results; i.e., pillars appeared in the dark areas first, which reveals that lateral electrical force plays an

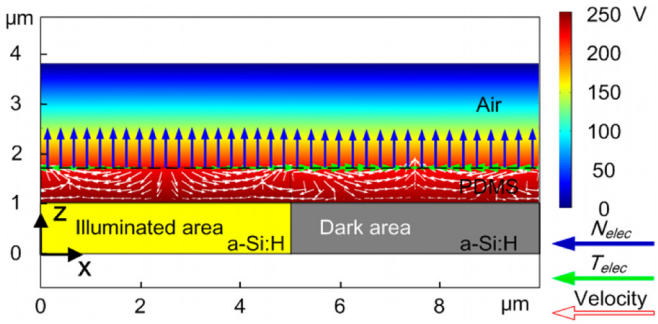

FIG. 7. Numerical simulation result showing the distribution of voltage, electric stresses ($N_{elec}$and T_{elec}), and velocity field according to the theoretical model. The relative permittivity of PDMS is 2.72 and the a-Si:H in illuminated and dark areas are 21.7 (assumed, see Ref. 25) and 11.7, respectively. The applied voltage between the two electrodes was 260 V. The density and viscosity of PDMS used in this simulation were 1030 kg/m^3 and 3.5 Pa s, respectively.

important role in the control of pillar nucleation sites in OEHI experiments as shown in Figures 2, 3, and 5.

In summary, we have demonstrated the formation of periodic and aperiodic pillar arrays on PDMS film by OEHI. Detailed experimental results and theoretical formulation with numerical analysis indicated the important role that the lateral electric force played in pillar growth and position control in OEHI. These results suggest that OEHI promises to be a rapid, low-cost and high-throughput method for generating micron-scale structures using polymer films.

The authors would like to express appreciation to researchers at the State Key Laboratory of Robotics, SIA, CAS, for their valuable discussions and support. This research work was partially supported by the National Natural Science Foundation of China (Project No. 61107043), the CAS-Croucher Joint Lab Scheme (Project No. 9500011), and the CAS FEA International Partnership Program for Creative Research Teams.

[1]Z. H. Nie and E. Kumacheva, Nat. Mater. **7**(4), 277 (2008).
[2]H. W. Li, B. V. O. Muir, G. Fichet, and W. T. S. Huck, Langmuir **19**(6), 1963 (2003).
[3]S. A. Jenekhe and X. L. Chen, Science **283**(5400), 372 (1999).
[4]E. Schaffer, T. Thurn-Albrecht, T. P. Russell, and U. Steiner, Nature **403**(6772), 874 (2000).
[5]S. Y. Chou and L. Zhuang, J. Vac. Sci. Technol. B **17**(6), 3197 (1999).
[6]P. Deshpande, L. F. Pease, L. Chen, S. Y. Chou, and W. B. Russel, Phys. Rev. E **70**(4), 041601 (2004).
[7]E. Schaffer, T. Thurn-Albrecht, T. P. Russell, and U. Steiner, Europhys. Lett. **53**(4), 518 (2001).
[8]Z. Q. Lin, T. Kerle, S. M. Baker, D. A. Hoagland, E. Schaffer, U. Steiner, and T. P. Russell, J. Chem. Phys. **114**(5), 2377 (2001).
[9]C. Y. Lau and W. B. Russel, Macromolecules **44**(19), 7746 (2011).
[10]Z. Q. Lin, T. Kerle, T. P. Russell, E. Schaffer, and U. Steiner, Macromolecules **35**(10), 3971 (2002).
[11]L. F. Pease and W. B. Russel, J. Chem. Phys. **118**(8), 3790 (2003).
[12]N. Wu and W. B. Russel, Nano Today **4**(2), 180 (2009).
[13]P. Deshpande, X. Y. Sun, and S. Y. Chou, Appl. Phys. Lett. **79**(11), 1688 (2001).
[14]S. Srivastava, P. D. S. Reddy, C. Wang, D. Bandyopadhyay, and A. Sharma, J. Chem. Phys. **132**(17), 174703 (2010).
[15]A. Atta, D. G. Crawford, C. R. Koch, and S. Bhattacharjee, Langmuir **27**(20), 12472 (2011).
[16]S. Grilli, V. Vespini, and P. Ferraro, Langmuir **24**(23), 13262 (2008).
[17]P. S. G. Pattader, I. Banerjee, A. Sharma, and D. Bandyopadhyay, Adv. Funct. Mater. **21**(2), 324 (2011).
[18]F. Wang and W. J. Li, "Optically Induced Electrohydrodynamic Instability-Based Micro-Patterning of Fluidic Thin Films," Microfluidics and Nanofluidics (published online).
[19]K. A. Leach, Z. Q. Lin, and T. P. Russell, Macromolecules **38**(11), 4868 (2005).
[20]A. Oron, S. H. Davis, and S. G. Bankoff, Rev. Mod. Phys. **69**(3), 931 (1997).
[21]D. A. Saville, Annu. Rev. Fluid Mech. **29**, 27 (1997).
[22]J. R. Melcher, *Continuum Electromechanics* (MIT Press, Cambridge, 1981), p. 3.18.
[23]H. A. Haus and J. R. Melcher, *Electromagnetic Fields and Energy* (Prentice Hall Englewood Cliffs, New Jersey, 1989), p. 6.7.
[24]J. R. Melcher, IEEE Trans. Educ. **17**(2), 100 (1974).
[25]N. A. Bakr, A. M. Funde, V. S. Waman, M. M. Kamble, R. R. Hawaldar, D. P. Amalnerkar, S. W. Gosavi, and S. R. Jadkar, Pramana **76**(3), 519 (2011).